

An apparatus to search for mirror dark matter via the invisible decay of orthopositronium in vacuum.

A. Badertscher^a A.S. Belov^b P. Crivelli^a M. Felcini^a
 W. Fetscher^a S.N. Gninenko^b N.A. Golubev^b M.M. Kirsanov^b
 L.L. Kurchaninov^c J.P. Peigneux^d A. Rubbia^{a,1} D. Sillou^d

^a*ETH Zürich, Zürich, Switzerland*

^b*Institute for Nuclear Research, INR Moscow, Russia*

^c*Institute of High Energy Physics, Protvino, Russia*

^d*CNRS-IN2P3, France*

Abstract

Mirror matter is a possible dark matter candidate. It is predicted to exist if parity is an unbroken symmetry of the vacuum. The existence of the mirror matter, which in addition to gravity is coupled to our world through photon-mirror photon mixing, would result in orthopositronium ($o - Ps$) to mirror orthopositronium ($o - Ps'$) oscillations. The experimental signature of this effect is the invisible decay of $o - Ps$ in vacuum.

This paper describes the design of the new experiment for a search for the $o - Ps \rightarrow$ invisible decay in vacuum with a sensitivity in the branching ratio of $Br(o - Ps \rightarrow$ invisible) $\simeq 10^{-7}$, which is an order of magnitude better than the present limit on this decay mode from the Big Bang Nucleosynthesis. The experiment is based on a high-efficiency pulsed slow positron beam, which is also applicable for other experiments with $o - Ps$, and (with some modifications) for applied studies. Details of the experimental design and of a new pulsing method, as well as preliminary results on requirements for the pulsed beam components are presented. The effects of $o - Ps$ collisions with the cavity walls as well as the influence of external fields on the $o - Ps \rightarrow o - Ps'$ oscillation probability are also discussed.

Key words: orthopositronium, invisible decay, mirror dark matter, pulse positron beam

¹ contactperson, e-mail address: Andre.Rubbia@cern.ch

1 Introduction

The dark matter problem provides one of the strongest indications for physics beyond the Standard Model. Although the unknown physics is usually addressed in a direct manner in high energy experiments, new results may also be expected from precision experiments at lower energies.

Orthopositronium ($o - Ps$, the triplet e^+e^- -bound state), is a particularly interesting system for such an approach [1-3]. For example, it has been shown recently that experiments searching for *invisible* decays of $o - Ps$ with the (currently achievable) level of sensitivity in the branching ratio $Br(o - Ps \rightarrow invisible) \simeq 10^{-8} - 10^{-9}$ have significant discovery potential [2]. An observation of $o - Ps \rightarrow invisible$ decay would unambiguously signal new physics phenomenon which could be induced either by the existence of extra dimensions [4], or of fractionally charged particles [5-7], or of light gauge bosons [2]. Other interesting experiments with $o - Ps$ are motivated by tests of high order QED corrections to the $o - Ps$ decay rate [8], searching for a violation of fundamental symmetries in positronium annihilation [9], tests of antimatter gravity in the free gravitational fall of positronium [10], the possibility to observe positronium Bose-Einstein condensation [11] and others. Among them the most exciting one is probably related to the search for the dark matter of a mirror-type.

Mirror matter is predicted to exist if parity is an unbroken symmetry of nature. The idea was originally discussed by Lee and Yang [12] in 1956, who suggested that the transformation in the particle space corresponding to the space inversion $\mathbf{x} \rightarrow -\mathbf{x}$ should not be the usual transformation P , but PR , where R corresponds the transformation of a particle (proton[12]) into a reflected state in the mirror particle space. After observation of parity nonconservation Landau assumed [13] that $R=C$, i.e. he suggested to identify antiparticles with the mirror matter, but then CP must be conserved which we know is not the case. The idea was further developed by A. Salam [14], and was clearly formulated in 1966 as a concept of the Mirror Universe by Kobzarev, Okun and Pomeranchuk [15]. In this paper it was shown that ordinary and mirror matter can communicate predominantly through gravity and proposed that the mirror matter objects can be present in our universe.

Since that time the mirror matter concept has found many interesting applications and developments. In 1980 it has been boosted by superstring theories with $E_8 \times E'_8$ symmetry, where the particles and the symmetry of interactions in each of the E_8 groups are identical. Hence, the idea of mirror matter can be naturally accommodated. Today's mirror matter models exist in two basic versions. The symmetric version proposed early was further developed and put into a modern context by Foot, Lew and Volkas [16]. The asymmetric version was proposed by Berezhiani and Mohapatra [17]. More detailed discussions of

mirror matter models can be found in Ref.[18].

In the symmetric mirror model the idea is that for each ordinary particle, such as the photon, electron, proton and neutron, there is a corresponding mirror particle, of exactly the same mass as the ordinary particle. The PR operator interchanges the ordinary particles with the mirror particles so that the properties of the mirror particles completely mirror those of the ordinary particles. For example the mirror proton and mirror electron are stable and interact with the mirror photon in the same way in which the ordinary proton and electron interacts with the ordinary photons. The mirror particles are not produced in laboratory experiments just because they couple very weakly to the ordinary particles. In the modern language of gauge theories, the mirror particles are all singlets under the standard $G \equiv SU(3) \otimes SU(2)_L \otimes U(1)_Y$ gauge interactions [16]. Instead the mirror particles interact with a set of mirror gauge particles, so that the gauge symmetry of the theory is doubled, i.e. $G \otimes G$ (the ordinary particles are, of course, singlets under the mirror gauge symmetry)[16]. Parity is conserved because the mirror particles experience $V + A$ (i.e. right-handed) mirror weak interactions while the ordinary particles experience the usual $V - A$ (i.e. left-handed) weak interactions.

It was realized some time ago by Glashow[19], that the orthopositronium system provides a sensitive way to search for the mirror matter. Glashow's idea is that if a small kinetic mixing of the ordinary and mirror photons exists [21], it would mix ordinary and mirror orthopositronium, leading to maximal orthopositronium - mirror orthopositronium oscillations, see Figure 1. Since mirror $o - Ps'$ decays predominantly into three mirror photons these oscillations result in $o - Ps \rightarrow invisible$ decay in vacuum. Remember, that due to the odd-parity under C transformation $o - Ps$ decays predominantly into three photons. As compared to the singlet (1^1S_0) state (parapositronium), the small $o - Ps$ decay rate (due to the phase-space and additional α suppression factors) gives an enhancement factor $\simeq 10^3$, making it more sensitive to an admixture of this new interaction [2,3,20].

Photon-mirror photon kinetic mixing is described by the interaction Lagrangian density

$$L = \epsilon F^{\mu\nu} F'_{\mu\nu}, \quad (1)$$

where $F^{\mu\nu}$ ($F'_{\mu\nu}$) is the field strength tensor for electromagnetism (mirror electromagnetism). The effect of ordinary photon - mirror photon kinetic mixing is to give the mirror charged particles a small electric charge[16,19,21]. That is, they couple to ordinary photons with charge $2\epsilon e^2$.

² Note that the direct experimental bound on ϵ from searches for 'milli-charged' particles is $\epsilon \lesssim 10^{-5}$ [5,7].

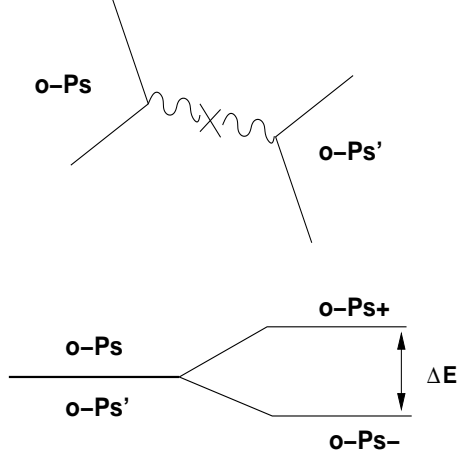


Fig. 1. The double degeneracy between orthopositronium mass eigenstates of ordinary o - Ps and mirror o - Ps' is broken when a small mixing (upper picture) term is included.

Orthopositronium is connected via a one-photon annihilation diagram to its mirror version ($o - Ps'$). This breaks the degeneracy between $o - Ps$ and $o - Ps'$ so that the vacuum energy eigenstates are $(o - Ps + o - Ps')/\sqrt{2}$ and $(o - Ps - o - Ps')/\sqrt{2}$, which are split in energy by $\Delta E = 2h\epsilon f$, where $f = 8.7 \times 10^4$ MHz is the contribution to the ortho-para splitting from the one-photon annihilation diagram involving $o - Ps$ [19]. Thus, the interaction eigenstates are maximal combinations of mass eigenstates which implies that $o - Ps$ oscillates into $o - Ps'$ with probability:

$$P(o - Ps \rightarrow o - Ps') = \sin^2 \omega t, \quad (2)$$

where $\omega = 2\pi\epsilon f$.

In the simplest case of $o - Ps \rightarrow o - Ps'$ oscillations in vacuum[19], because the mirror decays are not detected, this leads to an *apparent* increase in the decay rate, since the number of $o - Ps$, N satisfies

$$N = \cos^2 \omega t e^{-\Gamma_{sm} t} \simeq \exp[-t(\Gamma_{sm} + \omega^2 t)], \quad (3)$$

where $\Gamma_{sm} = 7.039934(10)\mu s^{-1}$ [22] is the Standard Model decay rate of $o - Ps$ (i.e. when the oscillation length goes to infinity). Thus $\Gamma^{eff} \approx \Gamma_{sm}(1 + \omega^2/\Gamma_{sm})$.

The above calculation is not applicable to an experiment, where the positronium is confined in a cavity, because in this case the collision rate is not zero and the loss of coherence due to the collisions must be included in the calculation of Eq.(3) [23,24]. Note, that the probability $P(o - Ps \rightarrow o - Ps')$ can also be affected by an additional splitting of $o - Ps$ and $o - Ps'$ states by an external

electric or magnetic field [23]. This is quite similar to the phenomenon of $n - \bar{n}$ [25] or muonium to antimuonium oscillations [26] in various environments, see section 2 for a discussion of these effects.

Recently, Foot discussed implications of the DAMA [27] and CRESST [28] experiments for mirror matter-type dark matter which is coupled to ordinary matter through the interaction of Eq.(1) [29] (for references related to mirror matter see e.g. [30]). He has shown that the annual modulation signal obtained by the DAMA/NaI experiment, as well as the CRESST data, can be explained by mirror matter-type dark matter if the photon-mirror photon mixing strength is in the region

$$\epsilon \simeq 4 \times 10^{-9} \quad (4)$$

Interestingly, this value of ϵ is also consistent with all other known experimental and cosmological bounds including SN1987a ³ and the standard Big Bang Nucleosynthesis (BBN) bound [33]. It is also in the range of naturally small ϵ -values motivated by grand unification models [18].

If ϵ is as large as in Eq.(4), the branching ratio $Br(o - Ps \rightarrow invisible)$ for invisible decays of orthopositronium in vacuum is of the order (see Section 4):

$$Br(o - Ps \rightarrow invisible) \simeq 2 \times 10^{-7} \quad (5)$$

For comparison, the BBN limits [33] deduced from the successful prediction of the primordial ⁴He abundance are

$$\epsilon < 3 \times 10^{-8} \quad (6)$$

and

$$Br(o - Ps \rightarrow invisible) < 10^{-5} \quad (7)$$

respectively.

The first experiment on the $o - Ps \rightarrow invisible$ decay, motivated by a puzzle in the $o - Ps$ decay rate (see below), was performed a long time ago [34], and then repeated with higher sensitivity [35]. The results exclude contributions to the $o - Ps$ decay rate from invisible decay modes (such as $o - Ps \rightarrow \nu\nu$, millicharged particles, etc..) at the level of $Br(o - Ps \rightarrow invisible) < 3 \cdot 10^{-6}$, but are not very sensitive to the $o - Ps \rightarrow o - Ps'$ oscillation mechanism because of the high collision rate in these experiments. Indeed the limit on ϵ extracted from the results of ref. [35], taking into account the suppression collision factor, is $\epsilon < 10^{-6}$ [23] and is not strong enough to exclude a possible mirror-matter contribution at the level comparable with the BBN limit of

³ The SN1987a limit $\epsilon < 10^{-9.5}$ obtained in Ref.[31] is actually much weaker. For a more detailed discussion of this constraint, see Ref.[32]

Eq.(6).

Given the indications for the mirror world coming from dark matter[29] and the neutrino physics [36,37], as well as the intuitive expectation that nature could be left-right symmetric, it is obviously important to determine experimentally whether orthopositronium is a window on the mirror world. Since there are no firm predictions for ϵ , experimental searches for $o-Ps \rightarrow invisible$ have to be performed with a sensitivity as high as possible. In particular, the question whether the sensitivity for the interesting branching ratio of Eq.(5) is experimentally reachable has to be studied.

The goal of this work is to present a design of the experiment for a search for $o - Ps \rightarrow invisible$ decay in vacuum with a sensitivity better than the corresponding BBN limit $Br(o - Ps \rightarrow invisible) < 10^{-5}$ and high enough to check the prediction of Ref.[29], $Br(o - Ps \rightarrow invisible) \simeq 2 \times 10^{-7}$. The experiment requires the production and subsequent decays of $o - Ps$'s to occur in vacuum [23,24], and hence, the use of a specially designed slow positron beam operating preferably in a pulsed mode to enhance the signal-to-noise ratio for the efficient tagging of $o - Ps$ production [38]. The experimental signature of $o - Ps \rightarrow invisible$ decay is the absence of an energy deposition which is expected from the ordinary o-Ps annihilation in a 4π calorimeter surrounding the positronium formation target. We show that this signature is clean and that the signal events can be identified with a high confidence level due to the efficient tagging of the positron appearance in the target and the high-efficiency measurement of its annihilation energy. It should be noted that recent substantial efforts devoted to the theoretical and experimental determination of the QED $o - Ps$ properties, hopefully results in a solution of the long-standing discrepancy between the measured and predicted orthopositronium decay rate in vacuum, see e.g. [39,40,41]. However, the current level of the theoretical precision achieved by Adkins et al. [8,22] is about two orders of magnitude better than the experimental one [40,41,42,43]. Thus, further positron beam based experiments to measure the $o - Ps$ decay rate in vacuum are required and are of great interest to test high-order QED corrections.

The paper is organized as follows. In section 2 we consider the $o-Ps \rightarrow o-Ps'$ oscillations and effects of various environments on it. In section 3 we report on the design of the experimental setup to search for the $o-Ps \rightarrow invisible$ decay in vacuum. The description of the detector components including the design of a high-efficiency pulsed positron beam is presented in sections 3 and 4. The preliminary simulation results and expected sensitivity level are discussed in sections 5 and 6, respectively. section 7 contains concluding remarks.

2 $o - Ps \rightarrow invisible$ decay rate in a vacuum cavity

In the simplest case of $o - Ps \rightarrow o - Ps'$ oscillations in vacuum [19] the branching ratio occurring during a long enough observation time can be calculated as

$$Br(o - Ps \rightarrow invisible) = \frac{2(2\pi\epsilon f)^2}{\Gamma_{sm}^2 + 4(2\pi\epsilon f)^2} \quad (8)$$

Eq.(8) may not be applicable to an experiment in a cavity. It is well known that collisions damp the oscillations, e.g. in the limit where the collision rate is much larger than the decay rate (or oscillation frequency, whichever is smaller) the effect of the oscillations becomes negligible. In addition, external fields might result in a loss of coherence due to additional splitting of mass eigenstates. Thus, their effect must be included [23,24].

Let us first consider the case where the collision rate is much larger than the decay rate, $\Gamma_{coll} \gg \Gamma_{sm}$ [24], then the evolution of the number of orthopositronium states, N , satisfies:

$$\frac{dN}{dt} \simeq -\Gamma_{sm}N - \Gamma_{coll}N\rho, \quad (9)$$

where the second term is the rate at which o-Ps oscillates into $o - Ps'$ (whose subsequent decays are not detected). In this term, ρ denotes the average oscillation probability over the collision time. That is,

$$\rho \equiv \Gamma_{coll} \int_0^t e^{-\Gamma_{coll}t'} \sin^2 \omega t' dt' \simeq \Gamma_{coll} \int_0^t e^{-\Gamma_{coll}t'} (\omega t')^2 dt', \quad (10)$$

where we have used the constraint that the oscillation probability is small, i.e. $\omega t \ll 1$. As long as $t \gg 1/\Gamma_{coll}$, a reasonable approximation for the vacuum cavity experiment, then

$$\rho \simeq \frac{2\omega^2}{\Gamma_{coll}^2}. \quad (11)$$

Thus, substituting the above equation into Eq.(9) we have

$$\Gamma^{eff} \simeq \Gamma_{sm} + \frac{2\omega^2}{\Gamma_{coll}} = \Gamma_{sm} \left(1 + \frac{2\omega^2}{\Gamma_{coll}\Gamma_{sm}} \right). \quad (12)$$

The difference between the higher decay rate measured in the vacuum cavity experiment, relative to the value predicted by theory, can be expressed as

$$\Gamma_{exp} - \Gamma_{sm} \simeq \frac{2\omega^2}{\Gamma_{coll}\Gamma_{sm}} \quad (13)$$

For the cavity size and the $o-Ps$ emission spectrum in a recent experiment on the $o-Ps$ decay rate in vacuum [42], we estimate that $\Gamma_{coll} \lesssim 3\Gamma_{oPs}$, which, neglecting the contribution from external fields (which are in fact negligible in this case[23]), implies that

$$\omega^2 \sim 2 \times 10^{-3} \Gamma_{oPs}^2 \Rightarrow \epsilon \lesssim 10^{-6}. \quad (14)$$

Thus, the limit of Eq.(14) is still not strong enough compared to the BBN one of Eq.(6).

In the presence of a static external electromagnetic field the $o-Ps - o-Ps'$ degeneracy is broken and the probability that positronium decays as mirror $o-Ps'$, rather than ordinary $o-Ps$, is

$$Br(o-Ps \rightarrow invisible) \simeq \frac{2(2\pi\epsilon f)^2}{\Gamma_{sm}^2 + 4(2\pi\epsilon f)^2 + \Delta^2} \quad (15)$$

where Δ represents an additional oscillations damping factor combining effects of collisions of $o-Ps$'s with the cavity walls, scattering on residual gas atoms and the influence of external fields [44].

Estimates obtained taking into account Zeemann and Stark effects in positronium and $o-Ps$ scattering in the Van der Waals potential of residual gas molecules in the cavity show that for the external magnetic field $\simeq 100$ G, the electric field $\simeq 100$ V and residual vacuum pressure $\lesssim 10^{-8}$ Torr, result in a value $\Delta < \Gamma_{sm}$ [44]. The most crucial parameter is the number N of $o-Ps$ collisions during its lifetime in the cavity, which gives a suppression factor $\simeq 1/N$. Hence N should be as small as possible, i.e. $N \leq 1$.

3 Experimental setup to search for the $o-Ps \rightarrow invisible$ decay

The experiment is designed with the goal to observe the $o-Ps \rightarrow invisible$ decays, if its branching ratio is greater than 10^{-7} . Figure 2 shows a schematic view of the experimental setup in which positrons from a pulsed beam [38] are stopped in the MgO target and either form positronium, i.e. $o-Ps$ or $p-Ps$, or annihilate promptly into 2γ 's. The secondary electrons (SE) produced by the positrons hitting the target are accelerated by the voltage applied to the target relative the grounded transport tube. Then they are transported by a magnetic field in the backward direction relative to the positrons moving in spirals along the magnetic field lines and deflected to a microchannel plate (MCP) by a $E \times B$ filter as is shown in Figure 3.

The trigger for data acquisition is generated by a coincidence within ± 3 ns

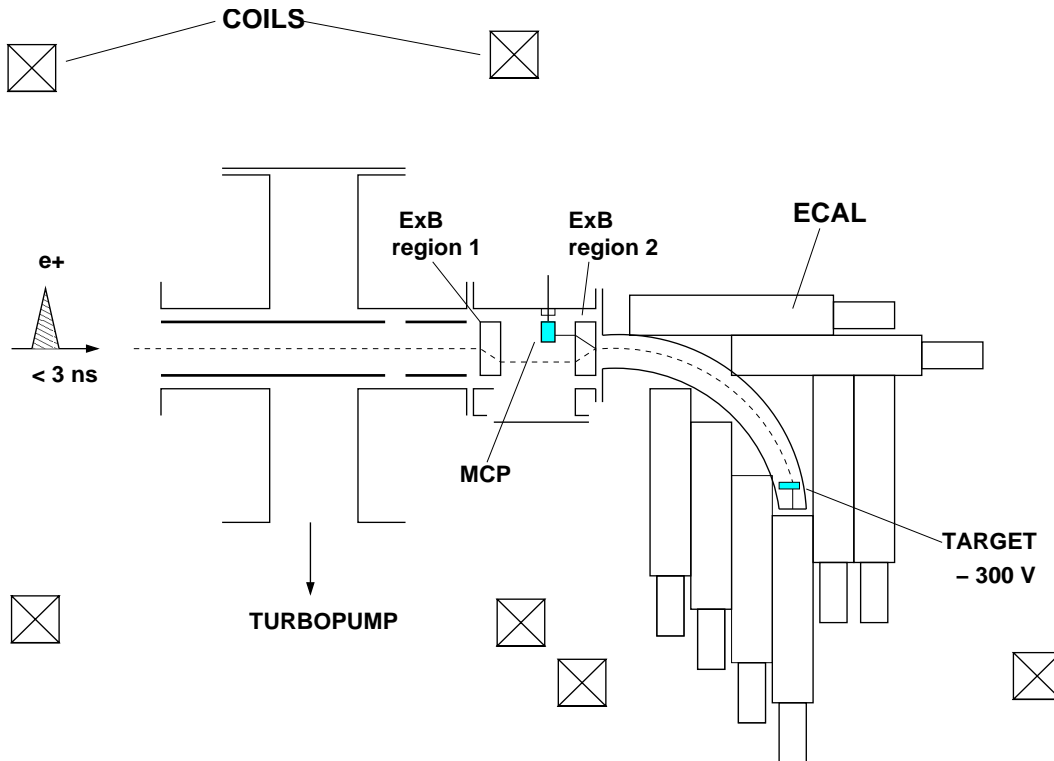


Fig. 2. Schematic diagram of the experimental setup.

of a pulse from the MCP and the signal from the pulsed beam, which is synchronized with the positron arrival time at the target.

Accordingly, the apparatus is designed with several distinct and separated parts: i) a pulsed slow positron beam and a low-mass target for efficient orthopositronium production in a vacuum cavity, ii) a positron appearance tagging system with a high signal-to-noise ratio based on a high performance MCP, iii) an almost 4π BGO crystal calorimeter (ECAL) surrounding the vacuum cavity for efficient detection of annihilation photons. The cavity has as little wall mass as possible to minimize photon energy absorption.

The occurrence of the $o-Ps \rightarrow o-Ps' \rightarrow invisible$ conversion would appear as an excess of events with energy deposition comparable with zero in the calorimeter above those expected from the prediction of the background. In case of a signal observation the number of excess events could be cross-checked by small variations of experimental conditions which affect the $o-Ps \rightarrow o-Ps'$ transition rate but do not result in a loss of energy from ordinary positron annihilations. The identification of signal events relies on a high-efficiency measurement of the energy deposition from the annihilation of positrons. Compared to the previous experiments on $o-Ps \rightarrow invisible$ decay, the use of the BGO calorimeter gives a significant reduction in total required ECAL mass (see section 3.3).

To achieve a sensitivity in the branching ratio of 10^{-7} in a reasonable amount of data-taking time, the rate of $o - Ps$ decays per second has to be as high as possible consistent with minimal reduction of the $o - Ps \rightarrow invisible$ signal efficiency and acceptably small dead time. For the pulsed positron beam design presented in Section 4, the trigger rate in the photon detector is expected to be $\simeq 100$ Hz which is low enough to allow these events to be recorded without losses.

3.1 Positron tagging system

The SEs produced by positrons hitting the $o - Ps$ production target are used to tag the time of positron appearance in the target. The positron tagging system is based on a high performance MCP as a SE detector. The low energy SE emerging from the target are accelerated by an electric field and deflected to the MCP by the $E \times B$ filter, as shown in Figure 2. The system works in detail as follows. The pulsed beam of positrons with energy $\simeq 500$ eV is guided by a magnetic field with a value of $B \simeq 100$ G and passes through a region with crossed electric and magnetic fields ($E \times B$ region 1 in the schematic diagram of Figure 2). The transversal electric field value is $E \simeq 500$ V/cm. Positrons drift in the crossed electric and magnetic fields with a velocity given by

$$V_d = E \times B / B^2 \quad (16)$$

For the given values of the electric and magnetic fields the drift velocity is $V_d = 7 \times 10^3$ m/s resulting in the positron displacement about of 11 mm in the drift region 1. The electric field in region 2 has the same value but the opposite direction relative to region 1. As a result, downstream of the region 2 positrons will move back to the axis if the transport system, separated from slow electrons and ions. Then, positrons are transported to the target in the curved magnetic field created by the coils. Preliminary results illustrating the method are shown in Figure 3, where the calculated trajectories of secondary electrons passing through the $E \times B$ filter are shown in the Y-Z plane for a wide primary positron beam. The energy spectrum of secondaries is taken from Ref.[45], the angular distribution is assumed to be isotropic.

The target is a disk with a diameter of $\simeq 10$ mm and a thickness of 0.1 mm. The SE acceleration potential of -300 V is applied to the target. The target surface is coated by MgO for an efficient production of orthopositronium and an efficient secondary electron emission [45]. The secondary electrons are transported in the backward direction relative to the positrons, see Figure 3, moving in spirals along the magnetic field lines. Thus, trajectories of the secondary electrons will be spatially separated from the positron trajectories by a distance estimated to be $\simeq 25$ mm, significantly larger than the diameter of the positron and the test electron beams ($\simeq 5$ mm). The MCP installed

between region 1 and region 2 (see Figure 2) detects the electrons. The background count rate of the MCP can limit the efficiency of the positron tagging. This and other sources of the background can be suppressed by an appropriate choice of the MCP type and by using a pulsed positron beam with a low duty cycle. The energy spectrum and the yield of SE are important for the tagging

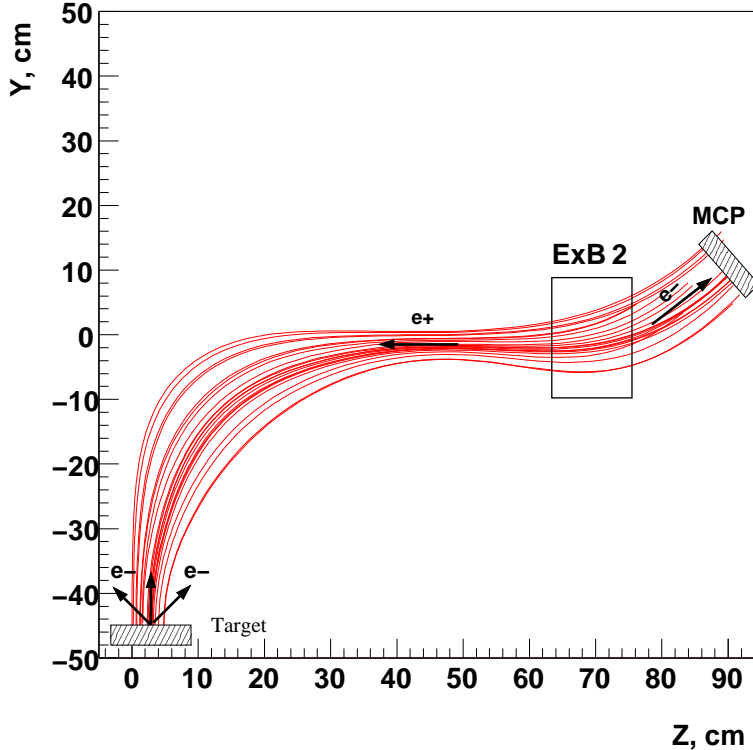


Fig. 3. Calculated trajectories of secondary electrons in the tagging system in Y - Z plane. The primary positron beam is increased in size for illustration purpose.

efficiency. The SE emission is a surface effect, involving only a very thin layer of the target material in the process. Thus, the SE yield and the MCP output signal are proportional to the energy loss dE/dx of positron. The SE are emitted with an energy up to 100 eV and a large angular spread. This results in a dispersion of their arrival time at the MCP. To reduce this effect the SE should be accelerated immediately after production by the electric field at the biased target. Note that the MCP pulse shape could be used for additional discrimination between the signals from positrons and the noise pulses.

The factors affecting the performance of the positron tagging system are

- the coefficient of secondary electron emission;
- the efficiency of the electron transport from the target to the MCP, and the efficiency of the MCP itself;
- the MCP noise level and the environmental background;
- physical backgrounds, from e.g. beam interactions with residual gas and cavity walls, with material of the $E \times B$ filters etc. accompanied by electron

or ion production.

We have selected the MCP Hamamatsu F4655-12 for the tagging system because it provides the best signal-to-noise ratio. The MCP signal rise time is $\simeq 300$ ps. The signal amplitude varies typically from 0.1 to 1 V depending on the applied voltage, the MCP gain and the number of the emitted SEs. The collection voltage between the MCP bottom surface and the anode is not critical, a setting above 100 V is sufficient for $> 95\%$ collection efficiency.

3.2 $o - Ps$ production target

A MgO coated film is planned to be used as $o - Ps$ production target. The production rate of $o - Ps$ per single positron is about 25 % at the positron energy of $\simeq 700$ eV [41]. The MgO is also reported to have the high secondary electron emission coefficient ($\gtrsim 4$) at this energy. Another possibility is a high porosity and low density SiO₂ target [42].

To ensure a minimal probability of total absorption of annihilation photons, the target itself and the surrounding components of the target region must be carefully designed. To minimize the thickness of dead material, in particular the thickness of the beam pipe in this region is very important. Based on simulation results a 1 mm thick Al pipe seems the best choice (see section 5). One possible way to avoid the problem of dead material is to drill a hole in the central crystal (Figure 2) and glue the beam pipe into it in such a way that the $o - Ps$ production and decay region is surrounded almost completely by the crystal active medium .

3.3 Photon detector

The optimal choice of the γ -detector (ECAL) can be made by the following considerations. The total ECAL mass W is given roughly by

$$W \simeq 4\pi/3\rho L^3 \tag{17}$$

where ρ and L are respectively mass density and the radius of the ECAL detector. We chose $L \simeq 20\lambda_{511}$, where λ_{511} is the attenuation length of 511 keV γ 's. The relevant parameters for different types of materials used in ECAL's are listed below in Table 1.

The required mass is minimal for a BGO ECAL due to its high effective Z (remember, the photo-absorption cross-section $\sigma \sim Z^5$). Another important

Table 1
Comparison between different types of ECAL.

| ECAL type | BGO | NaI | CsI(Tl) | Scintillator plastic/liquid |
|--------------------|-----------------------|------------------------|------------------------|--------------------------------|
| λ_{511} | $\simeq 1$ cm | $\simeq 2.5$ cm | $\simeq 1.9$ cm | $\simeq 10$ cm |
| density, g/cm^3 | 7.1 | 3.6 | 4.5 | 1.0 |
| ECAL mass, kg | $\simeq 240$ | $\simeq 1890$ | $\simeq 1034$ | $\simeq 33510$ |
| $N_\gamma/511$ keV | $\simeq 4 \cdot 10^3$ | $\simeq 20 \cdot 10^3$ | $\simeq 10 \cdot 10^3$ | $\simeq 2 \cdot 10^3$ |
| Hygroscopic | no | yes | slightly | no |

feature of BGO's is that they are not hygroscopic, thus, no additional dead material has to be introduced.

The schematic drawing of the γ -detector is shown in Figure 2. The γ -quanta produced in positron or positronium annihilation are detected by a (almost) 4π BGO crystal calorimeter [46]. We plan to use BGO crystals also for measuring of the photon time with respect to the arrival time, t_0 of the positron bunch on the target. The detector system consists of about 100 BGO crystal surrounding the vacuum beam pipe as shown in Figure 2. The full system is calibrated and monitored internally using the 511 keV annihilation line. For the crystal wrapped in aluminized mylar the light yield was measured to be 200 ± 14 photoelectrons/1 MeV. This results in a probability of zero energy detection due to Poisson fluctuation of the number of photoelectrons, to be less than 10^{-11} for the zero energy signal defined as events with energy deposition less than 50 keV [47,48]. This result justifies the selection of the BGO as the γ -detector. The crystals, which have been lent to us by the Paul Scherrer Institute (Villigen, Switzerland), have a hexagonal shape with a length of 20 cm and an outer diameter of 5.5 cm, their original wrapping is a 0.75 mm thick teflon. In order to reduce this amount of dead material, the inner ring of BGO's has been wrapped in a 2 μ m thick foil, aluminized from both side with 1000 Å thick layers. The required number of crystals, determined with the simulations, provides an almost isotropically uniform thickness of 20–22 cm of BGO.

4 High-efficiency pulsed positron beam

In this section we report the preliminary design of a high-efficiency pulsed slow positron beam for particle physics experiments with orthopositronium in vacuum. Our primary consideration is that the system should be of the magnetic transport type because this provides the simplest way to transport a

slow positron beam from the positron source to its target [51]. An electrostatic beam is also considered, but presently the problems with construction, time schedule and increased cost dominate over the benefits. The basic working principals involved in the design of magnetic or electrostatic variable-energy DC positron beams are well known [52]. The advantages and disadvantages of a beam formed and transported by a magnetic field in comparison to the electrostatic one are also known, see e.g. [53].

Various techniques to create pulsed positron beams have been reported with the main focus so far on material science applications [50]. Those attained by the Munich [54] and the Tsukuba [55] groups use RF power in the pulsed beam formation. However, acceleration by the sine function of the RF electric fields is by no means the optimal choice. The system based on this method requires a wide time window of chopping and accordingly the beam efficiency becomes small.

A pulsing system with a higher performance has recently been proposed by Oshima et al.[56]. The main idea is the same as for the RF method: to adjust the time-of-flight for each positron according to the time it arrives at the accelerating point. However, instead of applying a sinusoidal RF field, a more suitable pulse shape of the electric field is generated such as an approximate inverse parabol function of time [56]. This method has been further developed by Iijima et al [57] for the material measurements in which the lifetime or time-of-flight of orthopositronium atoms is close to the $o - Ps$ lifetime in vacuum $\simeq 142$ ns. For these applications it is necessary to modify the originally proposed technique [56] in order to generate higher intensity positron beams by accumulating positrons over a wider time span even though the bunch width becomes larger, but still much less than the typical measured timing intervals of $\simeq 100$ ns. By using a high permeability buncher core a bunch width of 2.2 ns (FWHM) for 50 ns collection time and a repetition period of 960 ns has been achieved [57]. The main problem encountered in this technique is the limitation of the voltage supplied by a post-amplifier to the buncher.

Our new pulsing method allows to compress an initial positron pulse of 300 ns to about 2 ns pulse width. The method relies on a positron velocity modulation by using a new double gap buncher technique. The detailed description of the system components as well as their requirements are presented.

4.1 Design criteria and overall system design

The beam is supposed to be used for several different experiments with $o - Ps$ in vacuum. Thus, the final beam construction should compromise several design goals which are crucial for them and which are summarized as follows:

- simple and not very costly experimental apparatus,
- beam energy range from 100 eV to 1000 eV,
- beam intensity of $\simeq 10^4 - 10^5$ positrons per second,
- pulse duration at the target $\delta t_T \lesssim 3$ ns for an initial pulse duration at the moderator $\delta t_M \simeq 300 - 400$ ns,
- repetition rate 0.3-1.0 MHz,
- high peak/noise ratio, (single) Gaussian shape of the pulse,
- beam spot size at the target position is of the order of a few millimeters assuming 3-5 mm ^{22}Na source diameter,
- minimal pumping time of the vacuum system,

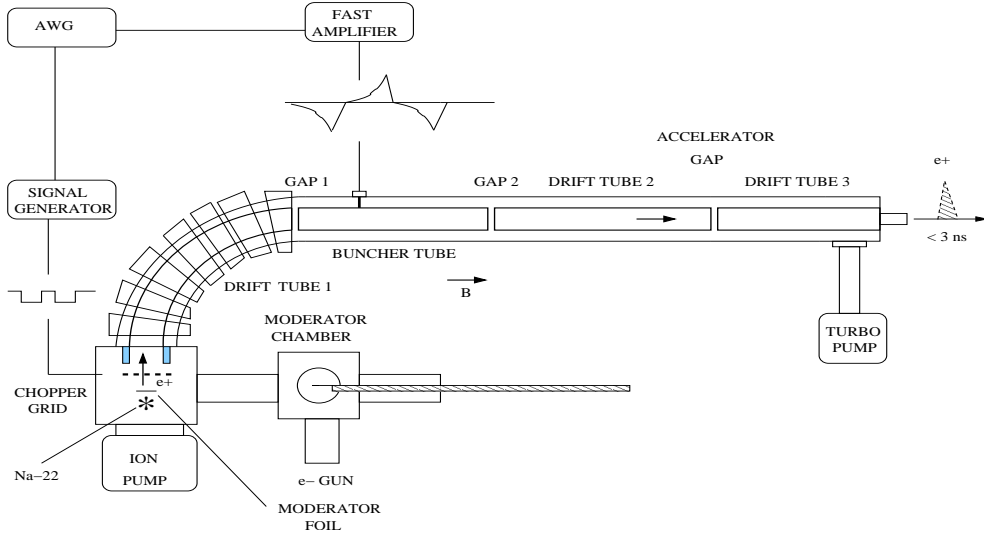


Fig. 4. Schematic illustration of the magnetically transported pulsed positron beam.

Figure 4 shows schematic illustration of the pulsed positron beam design. The positron pulsing section consists of a chopper and a buncher and is based on positron velocity modulation combined with the RF bunching technique. A positive potential ($\simeq 100$ eV) is applied to the moderator foil in order to insure the proper energy of the positrons at the buncher input. Initial positron pulses with duration 300 ns are formed with the chopper grid placed 2 mm apart from the moderator foil. The pulsed voltage with an amplitude about of +5V applied to the chopper grid relative the moderator foil will stop slow positrons with energy about 3 eV emitted from the moderator. Fast positrons emitted from the source are eliminated from the beam by the velocity analyzer (90 degrees curved solenoid, placed downstream the chopper). When the voltage applied to the chopper grid is zero, the positrons come through the chopper grid and are accelerated in the gap between the chopper grid and first drift tube (see Figure 4). Thus, positron pulses with a duration of 300 ns are produced by this way. The chopper voltage pulses can be produced by a standard fast-signal generator.

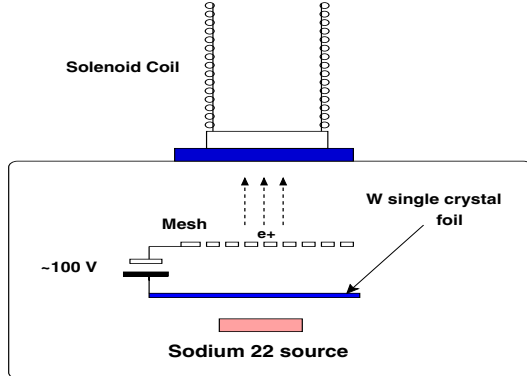


Fig. 5. Schematic illustration of the $W(100)$ single crystal moderator.

In the gap between the drift tube 1 and the buncher tube the velocity of positrons from the 300 ns pulse is modulated by a nonlinear pulsed voltage applied to the buncher tube relative to the drift tubes. The buncher tube length is determined by a distance-of-flight of positrons entering the buncher during 300 ns. In a second gap between the buncher tube and a drift tube 2 the positron velocity is modulated again by the same voltage pulse applied to the buncher.

The buncher voltage pulse is produced by an arbitrary waveform generator (AWG) connected to a fast post-amplifier. The pulse shape for the two-gap buncher is determined by calculations described in Section 3. In accordance with Liouville's theorem the compression ratio in this case is determined by the ratio of the final and initial energy dispersion in the positron beam pulse. Experimentally measured initial energy dispersion of the moderated positrons is about 2 eV (FW at 10% of maximum) [61]. Taking into account that the final energy spread in the given two gap buncher is about 200 eV we get the expected compression ratio of $\simeq 100$.

The moderation and associated voltages applied as shown in Figure 5 produce a positron beam which contains both moderated positrons with energy of about 3 eV and an unmoderated (β^+ decay energy) positron component which has to be rejected. There are several possibilities to build a positron velocity filter to select the slow, moderated component and reject high energy component from the source. We consider at the moment a simple bending filter, which is made of solenoidal coils positioned one after the other. Compensation of the beam drift due to the curved magnetic field is also foreseen.

The emittance of the beam is defined by the area in the phase space (r, α) multiplied by the square root of the energy and divided by a factor π , where r and α are the radial positron position and angle of the beam. The brightness of the beam B can be defined as [52] $B = \frac{I}{\phi^2 D^2 E}$, where I is the intensity, E

the particle energy, ϕ the angular divergence of the beam, and D the beam diameter. The brightness of the beam is limited by its initial emittance and by Liouville's theorem. This means that if the beam size is decreased, the angular divergence is increased. One of the problems is that positrons derived from the moderator will gain in emittance because of the presence of a transverse electric field in the vicinity of the moderator mesh, see Figure 5.

4.2 Analytical design of the pulsing system

To avoid the already mentioned over-voltage problem with the post-amplifier, we try first to design a simple pulsing system which accelerates and/or decelerates positrons only in a single gap during 300 ns, such that positrons arrive at the target after the buncher almost simultaneously. This problem can be solved exactly if all positrons at the entrance of the buncher have exactly the same longitudinal momentum. We use a time dependent electric field in the gap so that particles arriving first are decelerated and the later ones are accelerated. For a given distance from the gap to the target we have in this case one free parameter - the deceleration potential at the time $t = 0$. There is a soft limitation in the choice of the initial value of the deceleration potential: the momentum of positrons coming first should not be very small, since a small smearing of the initial momentum would cause a large dispersion in time at the target. However, we found the accelerating gap potential near the end of the 300 ns time interval should be more than 1 kV, which is difficult to achieve in a high frequency pulsed mode operation.

More convenient and economic is the buncher with two modulation gaps. In this case, as is shown in Figure 4, the buncher consists of the entrance drift tube 1, buncher electrode and exit drift tube 2. The decelerating or accelerating potential is applied to the buncher electrode with respect to the drift tubes resulting in positron velocity modulation in two gaps.

The simulations of the extraction optics, beam transportation and of the velocity modulation of positrons are performed with the GEANT4 [63] and 3D-Bfield [62] codes with the goal to minimize the timing resolution and optimize the shape of the bunching pulse.

The numerical solution for the shape of the buncher pulse is shown in Figure 6. It was calculated for the following characteristics of the system:

- moderated positrons have an average kinetic energy of $\simeq 3 \pm 0.5$ eV and are emitted isotropically from the flat film of 10 mm in diameter. According to the previous measurements [61] the low energy tail with intensity of 10% has been added,

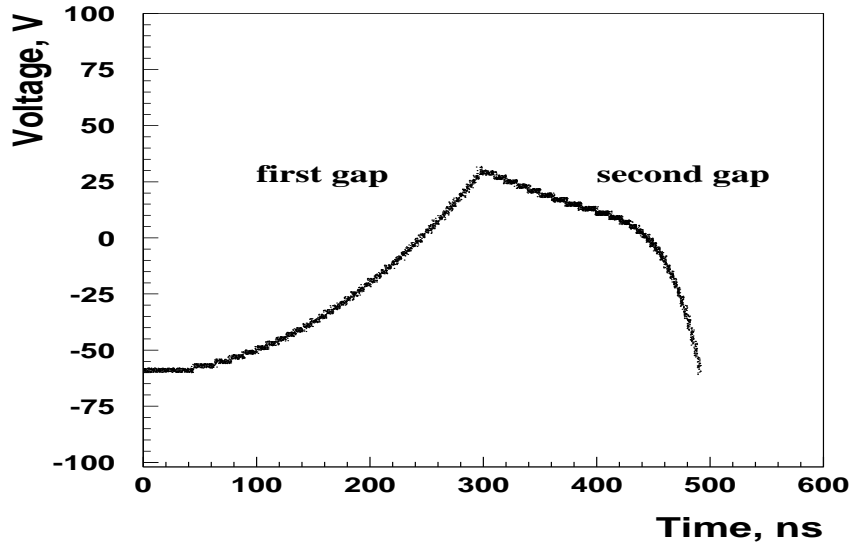


Fig. 6. *The bunching voltages seen by positrons at the first and the second velocity modulation gaps, respectively.*

- the velocity filter tube axis is curved with a radius of 45 cm. Particles enter into the tube along Y (upward) and exit along the Z axis,
- the buncher gaps are both 1 mm wide with the electric field along the Z axis.
- the buncher electrode is 140 cm long,
- the beam transportation tube is 1.05 m long and 10 cm in diameter

The optimal duration of the buncher pulse and the shape of the potential which positrons "see" in the gaps are chosen to satisfy the following criteria:

- the time difference between two positrons arriving at the gaps should be smaller at the second gap for the applied potential,
- the amplitude of the RF pulse should be within ± 60 V,
- after modulation at the second gap, positrons should arrive at the target at the same time.

We chose the parabolic time-dependent potential proportional to t^2 and changing from from -60 V (decelerating part) to 30 V for the positron velocity modulation at the first gap. Once this is fixed, the only free parameter left is the distance from the second gap to the target. The time dependence of the potential at the central electrode of the buncher at time $t > 300$ ns can then be calculated to make particles arriving at the target simultaneously. It is also assumed that the potential at the electrode at the end of the bunching pulse returns to its initial value -60 V. The pulse shape at the second gap is found

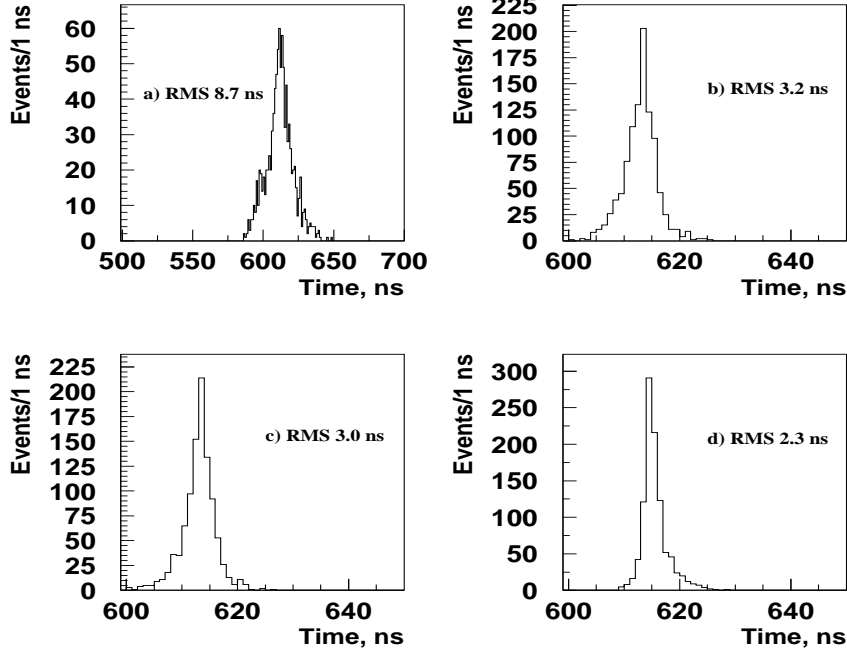


Fig. 7. Distribution of the positron time-of-flight at the target for the following cuts on the longitudinal energy $E_{||}$ of positrons emitted from the moderator: a) > 0 eV, b) > 1.5 eV c) > 2.0 eV and d) > 2.5 eV. The initial positron energy distribution is Gaussian with an average of 3 eV and $\sigma = 0.5$ eV, the angular distribution is taken to be isotropic.

as the result of an iteration procedure for the solution of the corresponding equations. Figure 6 shows the resulting shape of the bunching voltages seen by positrons at the first and the second velocity modulation gaps, respectively.

4.3 Requirements for the system components

The time shape of the positron pulse at the target is affected by the performance of the pulsed beam components. In this section requirements for the monochromaticity of the moderated positrons and for the amplifier used to generate the buncher pulse shown in Figure 6 are considered.

4.3.1 Monochromaticity of the moderated positrons

In Figure 7 the simulated positron time distribution at the target is shown for different energy spread of the initial positrons on the moderator. The degree

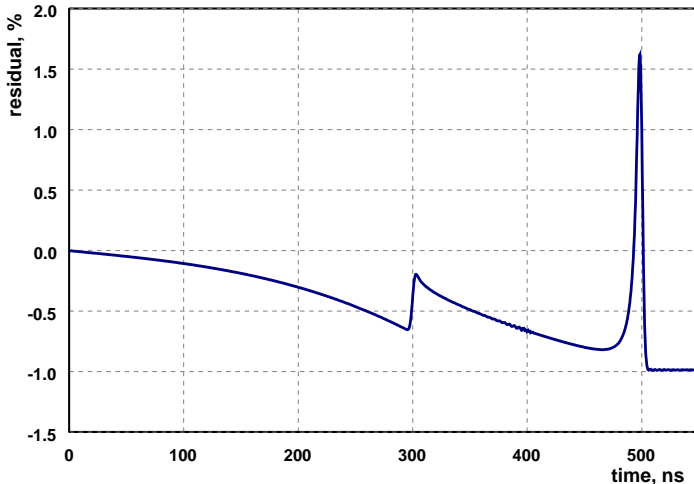


Fig. 8. Residual response of the post amplifier 100A250A for the input pulse shown in Figure 3.

of monochromaticity of the initial positrons was defined by the cuts on the longitudinal positron kinetic energy E_{\parallel} . The angular distribution of initial positrons was taken for simplicity to be isotropic. The results show that the best resolution achieved with this method is about 2 ns. The results also show that the quality of the moderator is an important parameter. So, the annealing of the W-foil *in situ* is important. Otherwise quick degradation of the surface quality through interactions with a gas results in a practically isotropic reemission of the positrons, and hence a significant increase in the phase space and timing spread.

4.3.2 Buncher pulse and amplifier response

The post-amplifier choice is made on the basis of the following requirements. We need an amplification factor of about 100 since the typical amplitude of an AWG (arbitrary waveform generator) is 1 V and the output signal has a peak to peak value of 90 V. The gain has to be programmable for final tuning of the output amplitude. The amplifier has to be sufficiently powerful to drive the 50 Ohm load. A few tens of Watts is expected for a typical signal rate. A wide frequency band from a few kHz to a few 100 MHz is required to minimize the signal shape distortions. And finally, the integral non-linearity has to be within at most 1% .

We select commercial RF post-amplifier 100A250A (Amplifier Research [64]) as a supplier of a fast pulse to the buncher. It has 100 W output power and a frequency bandwidth from 10 kHz to 250 MHz. It is designed for 50 Ohm

loading with reliable over-current and over-voltage protection.

The 100A250A post-amplifier is an AC-coupled device. To shift the signal baseline to the -60 V level, an external DC source is used. This voltage supplier is also used for fine pedestal tuning in order to compensate the baseline shift in the case of a high signal rate.

The response of 100A250A was simulated following the circuit characteristics. The output pulse shape differs from the input due to the finite frequency bandwidth. The residual shape is defined as $R(t) = S_{out}(t) - S_{in}(t)$ where $S_{in}(t)$ is the input signal supplied by AWG with unit amplitude and $S_{out}(t)$ is the amplifier output pulse calculated for unit gain. Figure 8 shows $R(t)$ expressed in percents of the input computed for the signal shape shown in Figure 6. The input shape is parameterized by an analytical function which has singularities (infinite first derivative) at $t = 300$ ns and $t = 500$ ns. Due to the upper frequency limit, the output signal is smoothed and differs from the input shape at these time points. This is indicated by two peaks on the residual plot. The post-signal baseline shift of about 1% is due to the lower frequency limit.

One can see that the overall deviation of the response is not more than about $\pm 1\%$. It is expected that this value will be better for real signals because the AWG can not reproduce the singularities of the theoretical shape. The simulations of the beam showed that 1% of signal deviation does not result in a significant distortion of the bunched positron pulse shape. The RMS of the corresponding distribution (see Figure 7, d) has been changed by less than 2%. However, for a deviation of the order of 5%, the RMS degrades from 2.3 to 2.8 ns. This means that the shape of the buncher pulse must be reproduced within about $\pm 1\%$ of the theoretical shape. This value seems to be achievable [64].

5 Monte Carlo simulations

The positron trajectories in the beam were simulated with the GEANT4 and the 3D-Bfield programs [62]. The $o - Ps$ production, propagation in the beam pipe, reflection on pipe walls and decay was simulated. The events for the $o - Ps \rightarrow 3\gamma$ process were generated taking into account the decay matrix element and assuming decays at rest.

The Monte Carlo simulation of the photon detection in the apparatus was based on the GEANT3 package [63]. The geometries of the beam transport pipe, photon detector, positron tagging system and its material were coded into simulations. The simulation results were also benchmarked with the re-

sults of our previous experiment on a search for the $o\text{-Ps} \rightarrow \gamma + X_1 + X_2$ decay mode [48]. In Figure 9, the distributions of the total energy deposited in 0.3 mm thick stainless steel pipe (upper plot) and in a 1 mm thick Al pipe are shown for the 2γ annihilation events. The γ -detection inefficiency was found to be less than 3×10^{-8} for the case of an Al pipe assuming that the zero-energy signal is defined as an event with the total energy deposition in the ECAL, $E \lesssim 100$ keV.

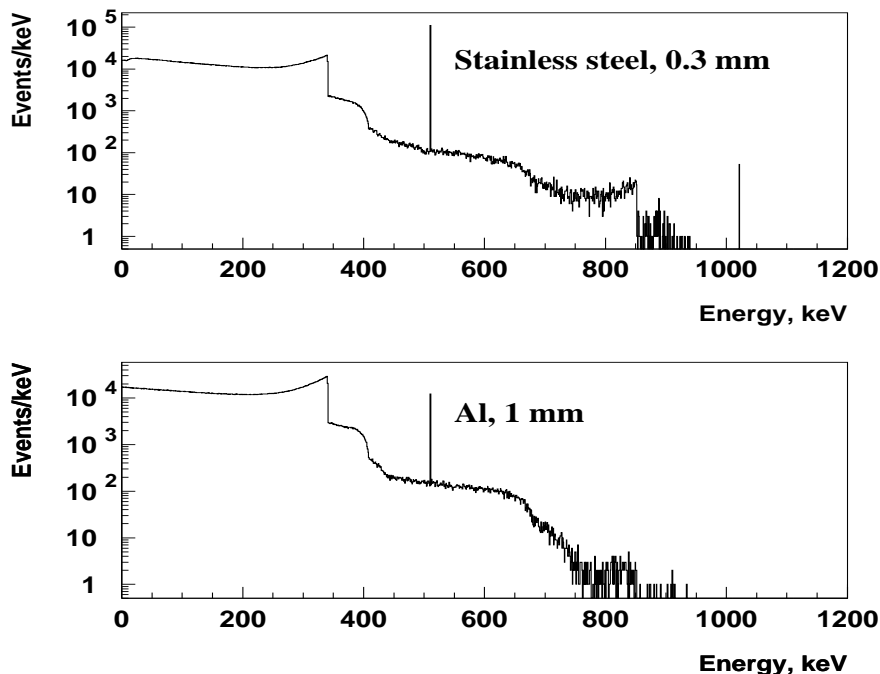


Fig. 9. Distributions of the energy deposited in a 0.3 mm thick stainless steel pipe (upper plot) and in a 1 mm thick Al pipe. The total number of simulated 2γ -events is 10^8 in both cases. The peaks at 511 keV and 1022 keV correspond to the total photo-absorption either of a single 511 keV photon or of both of them, respectively.

Simulations show that the main contribution to the γ -inefficiency comes from the total (due to photo-absorption) or fractional (due to Compton effect) photon energy loss in the material of the vacuum beam pipe. In the latter case, the energy deposition in the ECAL corresponds to a small amount of photoelectrons, so that the ECAL signal could be comparable with "zero-energy" due to statistical fluctuations. The γ -detection inefficiency due to the limited ECAL thickness is estimated to be less than 10^{-8} . A special mechanical design discussed in section 3.2 is necessary to reduce absorption in the pipe by choosing the appropriate materials and construction of the target region.

The energy spectrum of $o - Ps$'s produced at the MgO target is taken from

ref.[49]. The angular distribution is assumed to be isotropic and the intensity of the fast backscattered component [42] is taken to be 1% with a flat energy spectrum from 10 to 100 eV for a primary positron energy of a few keV. The collisional $o - Ps$ dissociation probability for a $o - Ps$ kinetic energy greater than 10 eV is taken to be 100%. The average number of $o - Ps$ collisions with the cavity walls during their lifetime in the cavity was estimated to be $N_{coll} \approx 2.5$, resulting in corresponding suppression factor in the sensitivity of the experiment (see sections 2,6). The other concerns are about $o - Ps$ decays near the entrance aperture to the detector, i.e. in the region of lower γ -detection efficiency, and the disappearance effect, namely when $o - Ps$'s escape the cavity region through the entrance aperture without being detected.

6 Sensitivity

The experimental signature of the $o - Ps \rightarrow invisible$ decay is an excess of events above the background at zero-energy deposition in the ECAL. The 90%-confidence level limit on the branching ratio for the $o - Ps \rightarrow invisible$ decay for a background free experiment is given by

$$S(90\%) = \frac{N(o - Ps \rightarrow invisible)}{N_{o-Ps} N_{coll}} \quad (18)$$

where $N(o - Ps \rightarrow invisible) = 2.3$ and the terms in the denominator are the integrated number of produced $o - Ps$'s (N_{o-Ps}), and the average number of $o - Ps$ collisions in the cavity, respectively. The number N_{o-Ps} is defined as a product $N_{o-Ps} = R_{e^+} \cdot \epsilon_{o-Ps} \cdot \epsilon_{e^+} \cdot t$, where the first factor is the number of delivered positrons per second on the target, the second one is the efficiency for $o - Ps$ production, and the third one is the efficiency of the secondary electron transportation from the target to the MCP in the positron tagging system. Taking $R_{e^+} = 2 \times 10^3/sec$, $\epsilon_{o-Ps} = 20\%$ and $\epsilon_{e^+} = 100\%$, we expect $\approx 7 \times 10^7$ prompt and $\approx 1.7 \times 10^7$ $o - Ps$ annihilations per day. Thus, $S(90\%) \simeq 10^{-7}$.

Eq.(18) gives the sensitivity for a background free experiment. We expect backgrounds which originates from the following sources: i) a fake positron tagging ii) the annihilation energy loss and iii) the disappearance effect. There are several sources of background that simulate the positron appearance signal:

- the MCP after-pulses or pulses produced due to ionization of the residual gas by passing positrons;
- cosmic rays;
- environmental radioactivity.

The MCP noise is typically low. Its level depends, e.g. on the ^{40}K contamination in the surrounding materials and on the intensity of penetrating photons,

although the sensitivity of the MCP to photons is quite low. However, for the purpose of this experiment the S/N ratio must be better than $\simeq 10^7$. To reach this level a high SE emission coefficient of the target combined with a good MCP energy resolution and a high $o - Ps$ production rate is crucial. A preliminary estimate shows that taking into account the noise spectrum of MCP4655-12 and the average number of secondary electrons per positron for the MgO target to be $N_{SE} \simeq 4$ [45], the MCP S/N ratio can be expected to be better than 10^5 . An additional noise suppression factor of $\simeq 100$ (at least) is expected from the use of the MCP signal in coincidence with the positron beam pulse [38] with the time resolution of $\simeq 3$ ns. The main source of beam associated background is expected from electrons and ions due to ionization of the residual gas atoms by positrons. Thus, a good vacuum is important. We estimate that with $R_{e^+} \simeq 10^3/s$ positrons on target, $\simeq 4$ secondaries per positron and a vacuum in the cavity of $\simeq 10^{-8}$ Torr, a MCP S/N ratio $> 10^7$ is achievable. The contribution from disappearance effect was also found to be small, $\lesssim 5 \times 10^{-8}$, although not completely free of assumption on fraction of fast $o - Ps$'s formed at the target. The preliminary overall background estimate results in $R_{bckg} \simeq 1.2 \text{ events/day}$.

In case of the observation of zero-energy events, one of the approaches would be to measure their number as a function of the residual gas pressure in the cavity. This would allow a good cross-check: relatively small variations of gas pressure results in larger peak variations at zero energy due to the damping of $o - Ps \rightarrow o - Ps'$ oscillations.

7 Summary

The design of our experiment to search for the $o - Ps \rightarrow \text{invisible}$ decay mode in vacuum has been presented. The sensitivity of the experiment to the branching ratio of the $o - Ps \rightarrow \text{invisible}$ decay in vacuum around $\simeq 10^{-7}$ seems to be achievable. Assuming that $o - Ps \rightarrow o - Ps'$ oscillations occur with mixing strength value $\epsilon \simeq 4 \times 10^{-9}$ a total number of $\simeq 100$ signal events would be expected in the ECAL during one month of data taking. Given that about 40 background events are expected a discovery with significance $\simeq 11$ could be possible [65].

One of the main features of the experiment is the use of a high-efficiency pulsed positron beam. The new proposed pulsing method allows to compress a 300 ns initial positron pulse into a pulse with < 3 ns width. This will allow to enhance the signal-to-noise ratio for the efficient tagging of $o - Ps$ production by more than an order of magnitude. A modification of the pulsing system could be made to use the beam for applications for material studies. Different components of the detector have to be constructed and fully simulated, in

order to test several crucial points of the design.

Acknowledgments

We express our thanks to Z. Berezhiani, R. Foot, S.L. Glashow, N.V. Krasnikov, V.A. Matveev and R. Mohapatra for many stimulating communications and discussions. The help and collaboration with N. Alberola (LMOPS), A. Gonidec, G. Roubout and J. Wolf from CERN, C. Wyon (CEA), and L. Knecht on DC beam prototype construction are greatly appreciated. We would like to thank Ph. Spälig (PSI) for the preparation of the ^{22}Na source, A. Skassirskaya (INR) for her help with the beam simulations and D. Taqqu (PSI) for his interest and useful discussions. Support of the Swiss National Foundation, ETH Zürich and Institute for Nuclear Research, Moscow is gratefully acknowledged.

References

- [1] Proceedings of Workshop on Positronium Physics, ETH Zürich, Zürich, Switzerland, 30-31 May 2003. To appear in *Int. J. Mod. Phys.*.
- [2] S. N. Gninenko, N. V. Krasnikov, A. Rubbia *Mod. Phys. Lett.* **A17**, 1713 (2002).
- [3] M. I. Dobroliubov, S. N. Gninenko, A. Yu. Ignatiev, V.A. Matveev, *Int. J. Mod. Phys.* **A8**, 2859 (1993).
- [4] S. N. Gninenko, N. V. Krasnikov, A. Rubbia *Phys. Rev.* **D67**, 075012 (2003).
- [5] S. Davidson, S. Hannestad, G. Raffelt, *JHEP* **0005**, 003 (2000); hep-ph/0001179.
- [6] M.I. Dobroliubov, A.Yu. Ignatiev, *Phys. Rev. Lett.* **65**, 679 (1990).
- [7] A.A. Prinz et al., *Phys. Rev. Lett.* **81**, 1175 (1998).
- [8] G. S. Adkins, R. N. Fell, J. Sapirstein, *Ann. Phys. (N.Y.)* **295**, 136 (2002).
- [9] P. A. Vetter, Contributed paper to Workshop on Positronium Physics, ETH Zürich, Zürich, Switzerland, 30-31 May 2003, to appear in *Int. J. Mod. Phys.*.
- [10] A.P. Mills Jr., M. Leventhal, *Nucl. Instrum. Meth.***B 192**, 102 (2002).
- [11] A.P. Mills Jr., *Nucl. Instrum. Meth.* **B 192**, 107 (2002).
- [12] T. D. Lee, C. N. Yang, *Phys. Rev.* **104**, 256 (1956).
- [13] L.D. Landau, *JETP* **32**, 405 (1957).
- [14] A. Salam, *Nuovo Cim.* **5**, 299 (1957).
- [15] I. Kobzarev, L. Okun, I. Pomeranchuk, *Sov. J. Nucl. Phys.* **3**, 837 (1966).
- [16] R. Foot, H. Lew, R. R. Volkas, *Phys. Lett.* **B272**, 67 (1991).

- [17] Z. Berezhiani, R. Mohapatra, *Phys. Rev.* **D62**, 6607 (1995);
See also, E. Akhmedov, Z. Berezhiani and G. Senjanović, *Phys. Rev. Lett.* **69**, 3013 (1992); Z. Berezhiani, A. Dolgov and R.N. Mohapatra, *Phys. Lett.* **B375**, 26 (1996); Z. Berezhiani, *Acta Phys. Pol.* **B 27**, 1503 (1996).
- [18] Z. Berezhiani, Contributed paper to Workshop on Positronium Physics, ETH Zürich, Zürich, Switzerland, 30-31 May 2003, to appear in *Int. J. Mod. Phys.*.
- [19] S.L. Glashow, *Phys. Lett.* **B167**, 35 (1986)
- [20] A. Rich, *Rev. Mod. Phys.* **53**, 127 (1981).
- [21] B. Holdom, *Phys. Lett.* **B166**, 196 (1986).
- [22] G. S. Adkins, R. N. Fell, J. Sapirstein, *Phys. Rev. Lett.* **84**, 5086 (2000).
- [23] S. N. Gninenko, *Phys. Lett.* **B326**, 317 (1994).
- [24] R. Foot, S. N. Gninenko, *Phys. Lett.* **B480**, 171 (2000).
- [25] V. A. Kuzmin, *JETP Lett.* **13**, 335 (1970);
K.G. Chetyrkin et al., *Phys. Lett.* **99 B**, 358 (1981).
- [26] G. Feinberg, S. Weinberg, *Phys. Rev.* **123**, 1439 (1961).
- [27] R. Bernabei et al. (DAMA Collaboration), *Riv. Nuovo Cimento.* **26**, 1 (2003);
astro-ph/0307403 and references there-in.
- [28] G. Angloher et al. (CRESST Collaboration), *Astroparticle Phys.* **18**, 43 (2002).
- [29] R.
Foot, hep-ph/0308254, and references therein; astro-ph/0309330, Contributed paper to Workshop on Positronium Physics, ETH Zürich, Zürich, Switzerland, 30-31 May 2003, to appear in *Int. J. Mod. Phys.*.
- [30] R. Foot, R. R. Volkas, *Phys. Rev.* **D68**, 021304 (2003); *Phys. Lett.* **B517**, 13 (2001); *Phys. Rev.* **D61**, 043507 (2000); *Phys. Rev.* **D52**, 6595 (1995);
A. Yu. Ignatiev, R.R. Volkas, *Phys. Rev.* **D68**, 023518 (2003); R. R. Volkas, hep-ph/9904437; Z. K. Silagadze, *Acta Phys. Polon.* **B33**, 1325 (2002); *Acta Phys. Polon.* **B32**, 99 (2001); *Mod. Phys. Lett.* **A14**, 2321 (1999); *Phys. Atom. Nucl.* **60**, 272 (1997); S. Blinnikov, astro-ph/9801015; astro-ph/9902305; astro-ph/9911138; R. N. Mohapatra, V. L. Teplitz, astro-ph/0004046; *Phys. Lett.* **B462**, 302 (1999); R. N. Mohapatra, S. Nussinov, V. L. Teplitz, *Phys. Rev.* **D66**, 063002 (2002); Z. Berezhiani, D. Comelli, F.L. Villante, *Phys. Lett.* **B503**, 362 (2001); L. Bento and Z. Berezhiani, *Phys. Rev. Lett.* **87**, 231304 (2001); L. Bento, Z. Berezhiani, *Fortsch. Phys.* **50**, 489 (2002); hep-ph/0111116; M. Yu. Khlopov et al., *Sov. Astron.* **35**, 21 (1991).
- [31] E. W. Kolb, R. N. Mohapatra, V. L. Teplitz, *Phys. Rev. Lett.* **77**, 3066 (1996).
- [32] R. Foot, A. Yu. Ignatiev, R. R. Volkas, *Phys. Lett.* **B503**, 355 (2001).
- [33] E. D. Carlson, S.L. Glashow, *Phys. Lett.* **B193**, 168 (1987).

- [34] G.S. Atojan, S.N. Gninenko, V.I. Razin, Yu.V. Ryabov, *Phys. Lett.* **B220**, 317 (1989).
- [35] T.Mitsui et al., *Phys. Rev. Lett.* **70**, 2265 (1993).
- [36] See, for example V. Berezinsky, M. Narayan, F. Vissani *Nucl. Phys.* **B658**, 254 (2003).
- [37] See for example, R. Foot, *Acta Phys. Polon.* **B 32**, 2253 (2001).
- [38] S. Gninenko, Contributed paper to Workshop on Positronium Physics, ETH Zürich, Zürich, Switzerland, 30-31 May 2003, to appear in *Int. J. Mod. Phys.*.
- [39] D. Sillou, Contributed paper to Workshop on Positronium Physics, ETH Zürich, Zürich, Switzerland, 30-31 May 2003, to appear in *Int. J. Mod. Phys.*.
- [40] S. Asai, O. Jinnouchi, T. Kobayashi, hep-ex/0308031; Contributed to Workshop on Positronium Physics, ETH Zürich, Zürich, Switzerland, 30-31 May 2003, to appear in *Int. J. Mod. Phys.*.
- [41] J. C. Nico, D. W. Gidley, A. Rich, P. W. Zitzewitz, *Phys. Rev. Lett.* **65**, 1344 (1990).
- [42] R. S. Vallery, P. W. Zitzewitz, D. W. Gidley *Phys. Rev. Lett.* **90**, 203402 (2003).
- [43] S. Asai, S. Orito, N. Shinohara, *Phys. Lett.* **B357**, 475 (1995).
O. Jinnouchi, S. Asai, T. Kobayashi, hep-ex/0011011.
- [44] S. N. Gninenko, N. V. Krasnikov, A. Rubbia, Paper in preparation.
- [45] R. Mayer, A. Weiss, *Phys. Rev* **B38**, 11927 (1988).
- [46] I.C. Barnett et al., *Nucl. Instrum. Meth.* **A455**, 329 (2000).
- [47] P. Crivelli, Contributed paper to Workshop on Positronium Physics, ETH Zürich, Zürich, Switzerland, 30-31 May 2003, to appear in *Int. J. Mod. Phys.*.
- [48] A. Badertscher et al., *Phys. Lett.* **B 542**, 29 (2002); hep-ex/0206054.
- [49] P. Sferlazzo, S. Berko, K. F. Canter, *Phys. Rev.* **B35**, 5315 (1987).
- [50] See for example, *Positron Beams and their applications*, ed. P. Coleman, World Sci. Publ. 2000.
- [51] N. B. Chilton, P. G. Coleman, *Meas. Sci. Technol.* **6**, 53 (1995).
- [52] P. Schultz and K. G. Lynn, *Rev. Mod. Phys.* **60**, 701 (1988).
- [53] R. S. Brusa et al., *Appl. Phys. Lett.* **77**, 1476 (2000).
- [54] P. Willutzki et al., *Meas. Sci. Technol.* **5**, 548 (1994), and references therein.
- [55] R. Suzuki, T. Ohdaira, T. Mikado, *Rad. Phys. and Chem.* **58**, 603 (2000), and references therein.
- [56] N. Oshima et al., *Appl. Surf. Sci.* **116**, 82 (1997).

- [57] H. Iijima et al., *Nucl. Instrum. Meth.* **A 482**, 641 (2002).
- [58] A. Belov et al., ETH Zürich, Internal Report, unpublished.
- [59] R. S. Brusa et al., *Appl. Surf. Sci.* **116**, 59 (1997).
- [60] W. E. Frieze, D. W. Gidley, K. G. Lynn, *Phys. Rev.* **B31**, 5628 (1985).
- [61] D. M. Chen, K. G. Lynn, R. Pareja, B. Nielsen, *Phys. Rev.* **B31**, 4123 (1985).
- [62] Code partly based on a package used for simulations of the Troitsk ν -mass experiment.
- [63] The simulation program is based on GEANT 4, CERN Program Library Long Writeup W5013.
- [64] www.amplifiers.com, private communications.
- [65] S.I. Bityukov, N.V. Krasnikov, *Mod. Phys. Lett* **A 13** 3235 (1998); *Nucl. Instrum. Meth.* **A 452**, 518 (2000).